

Identification of Herbig Ae/Be Stars in the Small Magellanic Cloud

Luke D. Keller , G. C. Sloan , Joana M. Oliveira , Kathleen E. Kraemer , Jacco Th. van Loon , Peter R. Wood, A. A. Zijlstra⁸, Joshua D. Simon, Rafael Ferreira, Martín Garay-MacLean, Jordan T. Hyatt¹⁰, Kevin Geidel, Joseph Quinn, Daniel Santoro¹, and Tori Knapp¹

Department of Physics and Astronomy, Ithaca College, Ithaca, NY, USA; lkeller@ithaca.edu ² Department of Physics and Astronomy, University of North Carolina, Chapel Hill, NC, USA Space Telescope Science Institute, Baltimore, MD, USA ⁴ Cornell Center for Astrophysics and Planetary Science, Cornell University, Ithaca, NY, USA ⁵ School of Chemical and Physical Sciences, Lennard-Jones Laboratories, Keele University, Staffordshire ST5 5BG, UK ⁶ Institute for Scientific Research, Boston College, Chestnut Hill, MA, USA ⁷ Research School of Astronomy and Astrophysics, Australian National University, Canberra, ACT, Australia The School of Physics and Astronomy, The University of Manchester, Manchester, UK

Observatories of the Carnegie Institution for Science, Washington, DC, USA ¹⁰ Department of Physics, New York University, New York, NY, USA Received 2018 December 22; revised 2019 May 7; accepted 2019 May 7; published 2019 June 24

Abstract

Protoplanetary disks orbiting intermediate-mass stars, Herbig Ae/Be stars, that have formed in a metal-poor environment may evolve differently than their Galactic cousins. A study of the planet-formation process in such an environment requires identification and characterization of a sample of candidates. We have observed several stars in the Small Magellanic Cloud, a nearby metal-poor dwarf galaxy, that have optical spectral properties of Herbig Ae/Be stars, including strong H α emission, blue continuum excess, and spectral types ranging from early G to B. Infrared spectra of these sources from the Spitzer Space Telescope show strong excess emission indicating the presence of silicate dust, molecular and atomic gas, and polycyclic aromatic hydrocarbons. We present an analysis of the likelihood that these candidates are Herbig Ae/Be stars. This identification is the necessary first step to future investigations that will examine the role of metallicity in the evolution of protoplanetary disks.

Key words: infrared: stars - Magellanic Clouds - protoplanetary disks - stars: variables: T Tauri, Herbig Ae/Be

1. Introduction

Star formation and subsequent planet formation depend on the chemical composition and evolution of gas and dust in dense molecular clouds and in circumstellar disks. Dust and gas characteristics also depend on the metallicity of the host galaxy. Some models predict higher cloud core masses and therefore more rapid formation and evolution of stars in metal-poor environments (Lamers et al. 1999; Lamers 2005; Leroy et al. 2009; Jameson et al. 2016). The lower metallicity implies a more primitive stage of galactic evolution—heavy element abundances in a galaxy increase as stars evolve and return products of nucleosynthesis to the interstellar medium (ISM) and this may have measurable effects on the dust-to-gas ratio (it should be lower), on abundances of molecular coolants (also lower), on dust grain size and composition, and on the transport of angular momentum within planet-forming disks. The stardisk interaction is also critical in regulating angular momentum. Higher total angular momentum is expected in more metal-poor environments (Ercolano & Clarke 2010), which may affect the timescales for planet formation.

Herbig Ae/Be (HAeBe) stars are the most massive stars $(2-10 M_{\odot})$ that are free of dense circumstellar envelopes as they approach the main sequence, so that their photospheres and circumstellar disks are usually unobscured and directly observable (Herbig 1960; Thé et al. 1986; Strom & Strom 1994). In metal-poor galaxies these stars should be more luminous than their Galactic counterparts because the lower dust abundance obscures them less, making them visible to us at earlier and more luminous stages of evolution (de Wit et al. 2003). Such systems in metal-poor galaxies may have

protoplanetary disks that evolve differently due to irradiation from their host stars with less shielding from dust. In order to test this theoretical scenario we need a sample of star-disk systems that have formed in a metal-poor environment. We have identified a population of candidate HAeBe stars in the metal-poor Small Magellanic Cloud (SMC), which is close enough to the Sun that the properties of individual stellar systems are observable for comparison to one another and to their Galactic counterparts. This paper describes our observational program to characterize these sources as HAeBe stars.

The SMC is a dwarf irregular galaxy located at a mean distance of 61.7 kpc from the Sun (Graczyk et al. 2014). Relative to the Milky Way, the SMC has lower abundances of heavy elements (one-fifth solar metallicity or Z = 0.004; Russell & Dopita 1992; Luck et al. 1998; Peimbert et al. 2000), relatively low internal extinction, high star formation activity, and an extinction curve and mid-infrared emission spectrum indicating a lower overall abundance of polycyclic aromatic hydrocarbons (PAHs) and dust in its ISM (Weingartner & Draine 2001; Li & Draine 2002; Sandstrom et al. 2012). Local dwarf irregular galaxies like the SMC are useful environments to study HAeBe stars and their protoplanetary disks because they are metal-poor relative to the Milky Way and still actively forming stars. A comprehensive study of planet formation in circumstellar disks, and how such protoplanetary systems orbiting intermediate-mass stars may be different in metal-poor environments relative to their Galactic counterparts, depends on the identification and detailed physical characterization of a representative sample of stars.

Many protoplanetary disk candidates have been identified in the SMC since Gatley et al. (1982) made the first identification

of a protostar there; however, very few have follow-up observations that identify all of the defining characteristics of HAeBe stars. Lamers et al. (1999), Beaulieu et al. (2001), and de Wit et al. (2003) identified seven pre-main-sequence (PMS) Ae and Be stars in the SMC by identifying stars with erratic optical variability and large $H\alpha$ equivalent widths. More recently the Spitzer Space Telescope has enabled mid-infrared studies of embedded higher-mass young stellar objects (YSOs; Simon et al. 2007; van Loon et al. 2010; Oliveira et al. 2011, 2013). Sheets et al. (2013) and Adams et al. (2013) identified 17 dusty OB stars in the SMC that have $H\alpha$ emission, which they suggest may be high-mass analogs to HAeBe stars. Kamath et al. (2014) identified 63 stellar sources in the SMC that appear to be intermediate-mass YSOs, of which 27 exhibit optical line emission, and 23 exhibit strong UV excesses. Testor et al. (2014) identified 12 massive YSO candidates in the H II region N26 in the SMC using infrared and optical imaging and spectroscopy. Ruffle et al. (2015) introduced a systematic method for classifying mid-infrared (MIR) point sources in the SMC, identifying 10 sources as candidate HAeBe stars (YSO-4 in their classification system) and Ward et al. (2017) recently obtained NIR spectra of 17 massive YSOs in the SMC identifying extended molecular hydrogen and Br γ emission, enabling a comparison of SMC and Galactic YSOs.

We have identified 13 candidate HAeBe stars, located in the SMC, selected in part because they are isolated or located at the fringes of (and therefore not embedded within) massive starforming regions. All of these sources have infrared colors resembling Galactic HAeBe stars. Six were previously identified by Oliveira et al. (2013) and Kamath et al. (2014) as possible intermediate-mass YSOs. We have acquired spectra in the $5-38 \,\mu m$ range using the Infrared Spectrograph (IRS) on the Spitzer Space Telescope as well as ground-based optical spectra. The infrared spectra show continuum and 10 μ m feature emission from warm silicate dust and high-contrast PAH emission features, which indicate direct irradiation of circumstellar material by stellar optical and ultraviolet (UV) radiation. Four show PAH emission, but lack strong $10 \, \mu \mathrm{m}$ silicate features, a combination observed in Galactic HAeBe stars (e.g., Keller et al. 2008, hereafter K08). In low-resolution optical spectra these sources have spectral energy distributions (SED) that clearly show stellar photospheres, 11 show H α in emission, and 11 show excess emission short of the Balmer jump. Taken together these properties are characteristic of HAeBe stars. While only one of our candidate HAeBe targets is located in a region of strong nebular emission in optical and infrared images, all are strong point sources in 24 μ m continuum *Spitzer* images (Bolatto et al. 2007). Strong dust-continuum emission combined with the H α emission and blue excess in most of our sources may indicate that the stars are actively accreting material from circumstellar protoplanetary disks.

In Section 2 we summarize our method of selecting sources, our follow-up spectroscopic observations, and our archival photometric data collection. Section 3 discusses results and our analysis leading to the conclusion that we have indeed identified a sample of HAeBe stars in the SMC. We summarize our conclusions in Section 4.

2. Observations

Our search began with a large sample of infrared point sources that we selected because their NIR and MIR colors fall

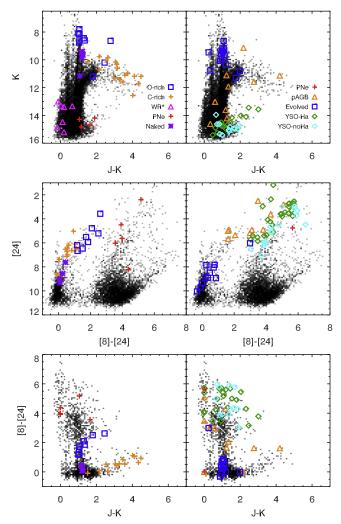


Figure 1. Color–magnitude and color–color diagrams of SMC targets observed in several research programs using the *Spitzer*-IRS. The subset of archival SMC targets with high-quality photometry are plotted in the left panels and the SMC-SPEC targets are plotted in the right panels. The gray-scale plots the S³MC point source catalog. Sources with positive identifications are indicated with colored symbols defined in the legend in the top panels.

in ranges overlapping those of Galactic HAeBe stars (Hernández et al. 2005), they are point sources in continuum-subtracted H α images, and are infrared point sources not embedded within intense infrared nebulosities. We have gathered mid-infrared spectra, optical spectra, and archival photometry spanning the optical to far-infrared for 17 of these objects.

2.1. Details of Source Selection

Our selection process begins with NIR and MIR color-magnitude and color-color diagrams (Figure 1). The underlying gray scale in all panels of Figure 1 represents the S³MC photometric measurements at 8 and 24 μ m (Bolatto et al. 2007) and in the $J\&K_s$ bands (2MASS; Skrutskie et al. 2006). The panels on the left show the individual sources that had been observed with the IRS in previous *Spitzer* campaigns at the time of our source selections. The right panels of Figure 1 contain the proposed targets for the SMC-SPEC program (IRS Guaranteed Time Observations in *Spitzer* Cycle 5: PI G. Sloan) and cover a broad range of source types for their larger study of the cosmic dust life cycle. In Figure 1 blue squares represent

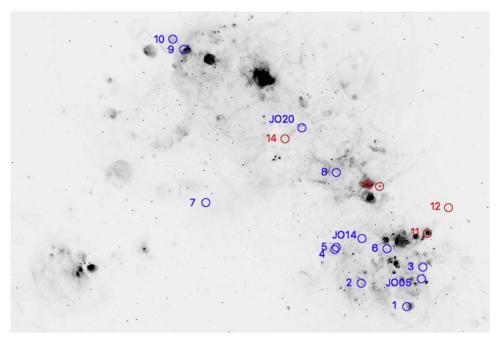


Figure 2. MCELS continuum-subtracted $H\alpha$ mosaic by Winkler et al. (2015). Blue circles indicate candidate HAeBe stars including three first identified by Oliveira et al. (2013); red circles are sources we have identified as planetary nebulae.

O-rich evolved sources (Kraemer et al. 2017; PI M. Egan, PID 3277) plus two O-rich evolved sources from Sloan et al. (2008); yellow/orange plus signs represent C-rich evolved sources from the Egan IRS sample (Sloan et al. 2006) plus one C-rich evolved source from Sloan et al. (2008); purple triangles represent Wolf–Rayet (WR) stars (PI C. Leitherer, PID 3185), chosen by the "WR" designation in their IRS target name. WR stars are generally much hotter and more luminous than HAeBe stars. Thick orange plus signs are planetary nebulae (PNe) identified in two Spitzer programs: PI J. Houck, PID 103, Bernard-Salas et al. (2009); and PI L. Stanghellini, PID 20443, Stanghellini et al. (2007). Purple asterisks represent naked stars identified with little or no dust emission in IRS spectra (PI J. Houck, PID 200, Sloan et al. 2008). Green diamonds are YSO candidates with H α detections. Blue diamonds are YSO candidates without H α . Orange triangles indicate post-AGB candidates as well as the three known post-AGB stars in the SMC (Kraemer et al. 2006). Blue squares indicate evolved-star candidates. Ruffle et al. (2015) provide a detailed description of the decision tree used to identify sources in the SMC-SPEC program: nonembedded SMC YSOs have low redshift (to distinguish them from active galactic nuclei), both atomic and molecular line emission, O-rich dust continuum emission (e.g., silicate), rising or flat 20–32 μ m SEDs, and either silicate feature emission or absorption. YSOs (indicated as such in Figure 1) fall in the ranges of $J - K_s = 0-3$ mag and [8]– [24] = 2-6 mag and have relatively bright 24 μ m magnitudes.

Next we identified the subset of sources that have $H\alpha$ emission using continuum-subtracted images from the Magellanic Cloud Emission Line Survey (MCELS; Smith & MCELS Team 1998; Winkler et al. 2015; Figure 2). For those sources that we identified as $H\alpha$ emission sources, we obtained follow-up MIR and optical spectra. The 17 sources that are both $H\alpha$ and MIR point sources and for which we have optical and MIR spectra form the sample we describe in the present analysis. Throughout this paper, in order to clearly distinguish the intermediate-mass sources we describe here from those

identified as high-mass YSOs by Oliveira et al. (2013), we refer to our targets as "candidate HAeBe stars" rather than YSOs. Three of our targets are sources originally identified by Oliveira et al. (2013) as possible HAeBe stars so we refer to them as SMC YSO n, where n refers to the Oliveira et al. (2013) target numbering system: these are SMC YSO 5, SMC YSO 14, and SMC YSO 20.

2.2. Spectroscopic Observations and Data Processing

Planetary nebulae (PNe), compact H II regions (CH II), and lower-luminosity post-asymptotic giant branch (pAGB) stars can have overlapping infrared colors with young stars hosting circumstellar disks, so our next step was to eliminate these source types from our sample using optical and infrared spectra. PNe and CH II have strong forbidden-line emission in the optical and infrared, which are generally missing or weaker in HAeBe stars, though there are some exceptions (e.g., Lamers et al. 1999).

2.2.1. Optical Spectra

We obtained optical spectra (Figure 3) using the Dual Beam Spectrograph at the Siding Springs Observatory 2.3 m telescope operated by the Australian National University (Rodgers et al. 1988). The effective resolution of the spectra is 3.8 Å (174 km s $^{-1}$). The spectrograph slit is 1.18 wide, which translates to 0.54 pc (1.1 \times 10 5 au) at $d_{\rm SMC}=61.7$ kpc. We used IRAF 11 data reduction and spectral extraction

We used IRAF¹¹ data reduction and spectral extraction routines and removed telluric features, but we still advise care in interpreting features in the regions of the A and B telluric bands (7590–7730 Å and 6860–6920 Å respectively). The spectra recorded with the red and blue channels in the Dual Beam Spectrograph are joined in the interval 6160–6300 Å so features in that range may be suspect as well. For slit spectra like these, nearby emission is subtracted as background, but the

¹¹ Image Reduction and Analysis Facility.

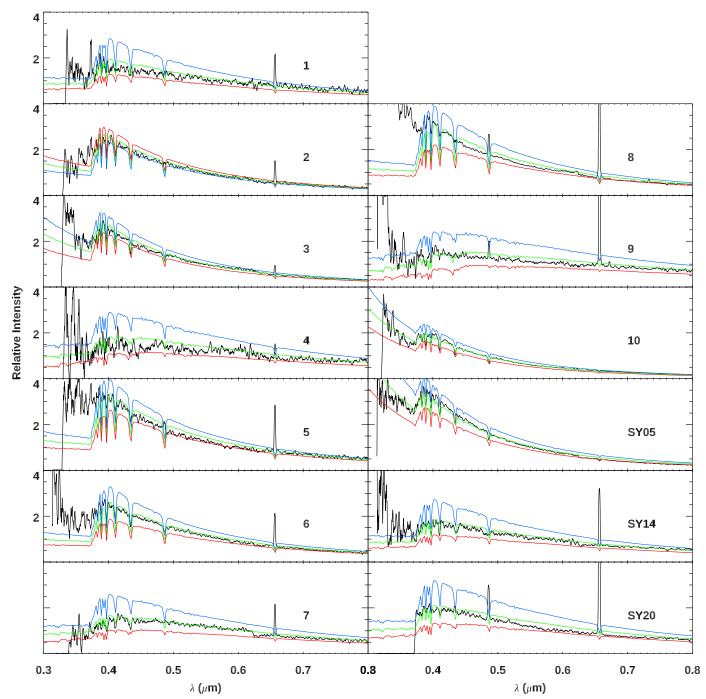


Figure 3. Optical spectra of our candidate HAeBe stars (black), corrected for interstellar reddening, with the best-fitting Kurucz model (green) superposed and bounded above and below, respectively, with hotter (blue) and cooler (red) models (typically $\pm 500-1000$ K, see Table 3). Because of the Balmer emission/veiling and blue–UV excesses expected for stars with protoplanetary disks, we obtain good model fits to the photospheric continuum, but not necessarily to the spectral features.

spatial variability of the background emission introduces some uncertainty so that nebular background (if present) could be under- or over-subtracted leaving apparent emission or absorption associated with the point source. We have used archival photometry (V magnitudes, see Table 1) to photometrically flux calibrate the optical spectra. We have applied reddening corrections to the spectra using A_V values (Table 3), for the locations in the SMC of each of our sources, that Rubele et al. (2018) derived from the VISTA Survey of the Magellanic Clouds (Cioni et al. 2011). Finally we use the extinction curve of Fitzpatrick (1999) to calculate and apply a reddening correction. This correction removes reddening due to

foreground extinction (Galactic and SMC) along the lines of sight to each of our sources. We are not able to estimate additional reddening from circumstellar extinction since we have no independent estimates of photospheric temperatures from which to gather color excesses.

Four of the sources in our sample, including the previously identified planetary nebula LHA 115-N 61 (Hajduk et al. 2014), have strong forbidden-line emission in their optical spectra (Figure 4). Thirteen of our sources have little or no forbidden-line emission in their spectra. Meatheringham & Dopita (1991) obtained optical spectra of PNe, and the four sources that we identify as PNe appear spectroscopically

 Table 1

 HAeBe Candidate Source List: Optical and Near-infrared Photometry

Target	S ³ MC ^a	U (mag)	B (mag)	V (mag)	I (mag)	J (mag)	H (mag)	$K_{\rm s}$ (mag)	Other ID
1	J004655.68-733158.43		19 ± 1	18.8 ± 0.7	17.9 ± 0.9	16.9 ± 0.3	15.7 ± 0.5	15.2 ± 0.2	b
2	J005054.18-732416.92		20.1 ± 0.1	19.5 ± 0.1	17.4 ± 0.9	16.2 ± 0.4	15.7 ± 0.2	14.9 ± 0.2	Hodge 108
3	J004542.95-731726.37	16.8 ± 0.1	17.3 ± 0.1	16.9 ± 0.1	16.8 ± 0.2	16.4 ± 0.1	16.1 ± 0.2	15.7 ± 0.1	
4	J005313.37-731217.56		20.3 ± 0.2	18.4 ± 0.1	17.4 ± 0.1	16.6 ± 0.2	15.8 ± 0.1	15.1 ± 0.1	WSHB 63
5	J005303.82-731137.46	17.3 ± 0.4	18.0 ± 0.2	17.8 ± 0.1	17.5 ± 0.5	16.8 ± 1.1	16.0 ± 0.1	15.4 ± 0.2	
6	J004849.03-731123.60	17.3 ± 0.1	17.4 ± 0.1	17.0 ± 0.1	16.6 ± 0.2	16.2 ± 0.4	15.5 ± 0.6	15.5 ± 0.3	
7	J010358.79-725532.52	18.0 ± 0.1	18.8 ± 0.1	17.7 ± 0.1	17.5 ± 0.5	16.9 ± 0.4	16.3 ± 0.5	15.6 ± 0.6	
8	J005313.56-724422.16	15.9 ± 0.1	16.6 ± 0.1	16.4 ± 0.1	15.7 ± 0.1	15.3 ± 0.1	15.0 ± 0.1	14.6 ± 0.1	LIN 238
9	J010528.62-715942.79	18.2 ± 0.1	19.1 ± 0.1	18.3 ± 0.1	17.1 ± 0.1	16.5 ± 0.1	15.8 ± 0.1	15.0 ± 0.1	b
10	J010619.56-715559.23	16.6 ± 0.1	17.4 ± 0.2	17.5 ± 0.1	16.9 ± 0.3	16.3 ± 0.2	15.5 ± 0.1	14.7 ± 0.2	b
SMC YSO 5	J004547.53-732142.10	15.8 ± 0.4	16.5 ± 0.1	16.5 ± 0.1	16.4 ± 0.2	16.2 ± 1.1	15.8 ± 0.7	14.9 ± 0.1	c
SMC YSO 14	J005058.09-730756.78	17.6 ± 0.1	17.2 ± 0.1	17.3 ± 0.1	16.6 ± 0.1	15.9 ± 0.2	15.3 ± 0.3	14.6 ± 0.2	c,b
SMC YSO 20	J005606.37-722828.05	17.6 ± 0.1	17.2 ± 0.1	17.3 ± 0.1	16.6 ± 0.1	15.6 ± 0.3	15.2 ± 0.1	14.2 ± 0.3	c
11	J004530.76-730455.84	15.6 ± 0.1	16.3 ± 0.1	16.1 ± 0.1	16.0 ± 0.1	15.7 ± 0.4	15.5 ± 0.4	14.8 ± 0.7	IRAS 00460
12	J004353.82-725514.87	15.9 ± 0.1	17.1 ± 0.1	17.2 ± 0.1	17.0 ± 0.1	16.6 ± 0.1	15.7 ± 0.1	14.4 ± 0.4	LIN 49
13	J004941.27-724848.56	14.8 ± 0.1	16.3 ± 0.1	16.1 ± 0.1	15.8 ± 0.1	15.5 ± 0.4	15.2 ± 0.3	14.9 ± 0.5	LkHa 115+32
14	J005730.06-723224.46	13.8 ± 0.1	14.7 ± 0.1	14.5 ± 0.1	15.2 ± 0.5	14.7 ± 0.3	14.5 ± 0.4	13.8 ± 0.7	LkHa 115+61

Notes. Data in this table are not corrected for extinction: UBV magnitudes are from MCPS; I magnitudes are an average of MCPS and DENIS; J and K_s magnitudes are an average of DENIS, IRSF, 2MASS, and 6MASS; H magnitudes are an average of IRSF, 2MASS, and 6MASS.

similar to theirs. We therefore interpret the strong forbiddenline emission present in this subset of our sample as an identifying characteristic of ionized gas in PNe or CH II regions and eliminate sources 11, 12, 13, and 14 from our list, leaving 13 candidate HAeBe stars.

One of our sources (#9) is located at the edge of a strong $H\alpha$ nebulosity, three others (#1, 2, and 8) are located on the fringes of faint $H\alpha$ emission nebulae, and the rest are isolated $H\alpha$ point sources (Figure 2), though faint $H\alpha$ emission is present at low levels throughout the MSELS image. The strong $H\alpha$ emission lines in all but two of the sources we have classified as HAeBe show a marked difference in widths relative to sources we have classified as PNe. Our HAeBe star candidates have $H\alpha$ full width at half maximum (FWHM) ranging from 5.5 to 9.3 Å, with a mean width of 6.6 Å (300 km s⁻¹). For the PNe the $H\alpha$ FWHM range from 4.1 to 4.9 Å, with a mean width of 4.6 Å (210 km s⁻¹).

2.2.2. Infrared Spectra

We used the low-resolution modules of the IRS on the Spitzer Space Telescope ($R = \lambda/\Delta\lambda \sim 90$), to obtain infrared spectra in the wavelength range 5–38 μ m (Figure 5). Sloan et al. (2015) described the IRS observations and the data reduction pipeline in detail. Briefly, we used version \$18.18 of the IRS pipeline from the Spitzer Science Center, removed the background from the spectral images by subtracting an image with the same source in a different nod position or aperture, and extracted the spectra. We calibrated the spectra using IRS spectra of the K giants HR 6348 and HD 173511 (Sloan et al. 2015), corrected each spectral order segment with scalar multiplication to remove discontinuities between them, and removed extraneous overlapping data at the ends of the spectral orders. We applied an optimal extraction algorithm following the approach of Lebouteiller et al. (2010). Projected widths of the IRS slits at the distance of the SMC are 1.1 pc $(2.3 \times 10^5 \text{ au})$

for the \sim 3."7 5–14 μm slit, and 3.2 pc (6.5 \times 10 au) for the \sim 10."6 14–38 μm slit.

Oliveira et al. (2013) used a decision tree, based primarily on infrared spectral features, to identify massive YSOs in the SMC, and later Ruffle et al. (2015) used this system to assess all of the IRS spectra toward the SMC. Their source-type identifications confirm ours when applied to our HAeBe candidates: of our 13 candidate HAeBe stars, 5 (2, 8, 9, SMC YSO 14, and SMC YSO 20) are in the YSO-4 category. These appear in Figure 5 as the sources with silicate emission features at 9.7 and 18 μ m. Another 6 of our candidate HAeBe stars (1, 3, 5, 6, 7, and 10) fall in the YSO-3 category with PAHs, and no silicate emission, combined with a flat or rising continuum. These sources are the least embedded of the identified YSOs but do not (yet) show atomic fine-structure lines indicating an H II region. We have classified the last two HAeBe candidates (4, and SMC YSO 05) as YSO-1 s, which show absorption from ices (Oliveira et al. 2013). All of our sources also show PAH emission at 6.2, 7.7, and 11.3 μ m. Besides the five SMC-SPEC sources we have identified as HAeBe candidates, Ruffle et al. (2015) classified three other SMC-SPEC spectra and two from another program (NGC 346 MPG 454 and 605) as YSO-4 s. We have not yet obtained optical spectra for these and thus do not include them in the present analysis.

2.3. Optical and Infrared Photometry

We obtained archival photometric data in the optical and NIR (Table 1) as well as in the MIR and far-infrared (FIR) (Table 2). For each source, we began a search using the field-of-view center coordinates observed by the IRS. In all but one case, we found the corresponding source in the 2MASS catalog (Two-Micron All-Sky Survey; Cutri et al. 2003; Skrutskie et al. 2006). The one exception was Massey SMC 20781 (our target 4), for which we used the position at 24 μ m in the SAGE-SMC survey (Gordon et al. 2011). Using these positions, we then

^a S³MC target designations contain equatorial coordinates in sexagesimal format: Jhhmmss.ss-ddmmss.ss.

b Sources identified by Kamath et al. (2014) as possible YSOs in their search for post-AGB/RGB candidates in the SMC.

^c Sources identified by Oliveira et al. (2013) as possible HAeBe stars in their study of embedded YSOs in the SMC.

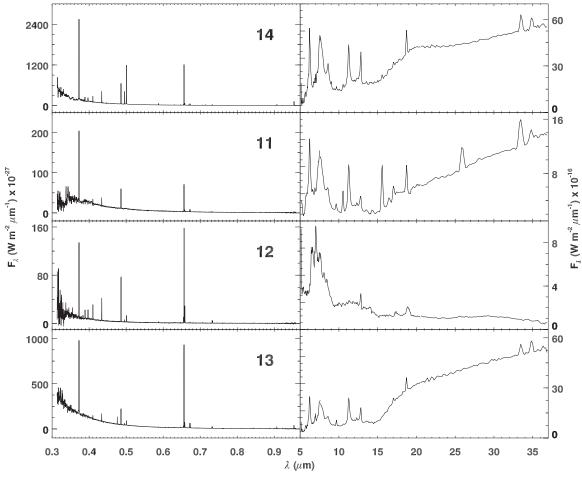


Figure 4. Optical (left) and infrared (right) spectral identification of planetary nebulae. The top panel is LHA 115-N 61, a target in our source list (#14) that was previously identified as a planetary nebula. The remaining three panels are sources in our sample that we have rejected as HAeBe candidates due to strong forbidden emission lines in both the optical and infrared spectra that resemble those in planetary nebulae and compact H II regions.

searched for more photometry using the Infrared Science Archive¹² and VizieR. ¹³

Optical photometry is from the Magellanic Clouds Photometric Survey (MCPS; Zaritsky et al. 2002), covering UBVI, with additional I-band photometry from the Deep NIR Survey of the Southern Sky (DENIS; Cioni et al. 2000). We collected JHK_s photometry from several sources: 2MASS, which also obtained a deeper survey of the SMC (2MASS-6X; Skrutskie et al. 2006); DENIS; and data from the Infrared Survey Facility (Kato et al. 2007). Mid-infrared photometry is from the SAGE-SMC survey, which includes data for three epochs and includes the smaller S³MC survey in the core of the SMC.¹⁴ We also used data from the Wide-field Infrared Survey Explorer (WISE; Wright et al. 2010) and the reactivated WISE mission to continue the hunt for Near-Earth Objects (NEOWISE-R; Mainzer et al. 2014). Far-infrared photometry came from the HERITAGE survey (Herschel Inventory of the Agents of Galactic Evolution; Meixner et al. 2013). For each source the photometry listed in Tables 1 and 2 for a given filter is the average—by catalog and epoch for catalogs containing multiepoch entries—of all data available for that filter. We have applied a reddening correction to the UBVIJHK_s photometry using the same method as with

our optical spectra (Section 2.2.1). We present uncorrected magnitudes in Table 1.

3. Discussion

Our observations have enabled us to identify a sample of candidate HAeBe stars that share several properties: all but one (see Section 3.2.5) are point sources at all wavelengths and spatial resolutions thus far observed (blue through far-infrared); they have strong Balmer-line emission, but weak or no optical forbidden-line emission; they have strong infrared excess emission due to dust and PAHs. Many have strong excess emission on the blue side of the Balmer jump. None are embedded in dense nebulosity; they are spatially isolated from (though some are located near) bright star-forming regions. All of these are common characteristics of Galactic HAeBe stars. We now turn to a discussion of the physical properties of these systems as determined from our observations.

3.1. Host Star Properties from Optical Spectra and Photometry

We have estimated the physical characteristics for the host stars of our HAeBe candidates using optical data. The spectral resolution and signal-to-noise ratio (S/N) are not sufficient in all of our optical spectra to systematically determine temperatures from spectral line strengths and ratios alone (e.g., Kamath et al. 2014) so we have iteratively fit the Rayleigh–Jeans

¹² IRSA: http://irsa.ipac.caltech.edu.

¹³ Harvard portal: http://vizier.cfa.harvard.edu.

¹⁴ Spitzer Survey of the Small Magellanic Cloud; Bolatto et al. (2007).

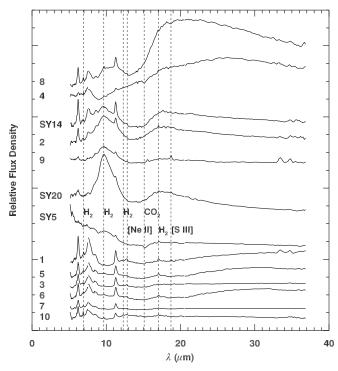


Figure 5. Spitzer IRS spectra of our candidate HAeBe stars in F_{λ} and offset vertically for separation and easy comparison. SY5, SY14, and SY20 refer to sources SMC YSO 5, SMC YSO 14, and SMC YSO 20 respectively.

continua in our spectra to stellar photospheric models (Castelli & Kurucz 2003) generated for main-sequence stars with metallicity nearest the SMC value of Z = 0.004 (Russell & Dopita 1992; Luck et al. 1998; Peimbert et al. 2000). The photospheric models have luminosity class V, $\log g = 4.0$, and Z = 0.006 ([M/H] = -0.5). In Figure 3 we have plotted the best-fit Castelli & Kurucz models overlaid with the respective optical spectra of our 13 HAeBe candidate sources. We visually estimated uncertainties in our effective temperatures by plotting models that are hotter and cooler than the best fit, also shown in Figure 3. The continuum fitting focuses on regions of the spectra that we expect to be purely photospheric continuum at our spectral resolving power: 4400-4800 Å, 5000–6000 Å, and 6700–7800 Å. This avoids the Balmer lines and the blue end of the spectra where the S/N is lower and where several sources show excess emission. Table 3 lists effective temperatures derived from this analysis.

We tested this method of estimating temperatures by applying it to spectra for a sample of Galactic stars in the XSHOOTER library for which spectral types have been determined independently (Chen et al. 2014). The test stars range from spectral type G to O and are on or near the main sequence. Our temperature estimates match the derived spectral types of Chen et al. (2014) giving us high confidence that our continuum fitting method for estimating photospheric temperatures is accurate to within our estimated uncertainties (Table 3). However, because the reddening corrections we applied to the HAeBe candidate spectra (prior to determining photospheric temperatures) do not include circumstellar extinction, our temperature estimates for those sources are lower limits.

We have calculated bolometric luminosities (Table 3) from dereddened V-band magnitudes using a distance of $d_{\rm SMC}=61.7$ kpc and luminosity class V bolometric corrections from Kenyon & Hartmann (1995). In Figure 6 we plot our

candidate HAeBe star luminosities and effective temperatures in a Hertzsprung–Russell diagram (HRD) with PMS and main-sequence model isochrones and evolutionary tracks calculated by Tognelli et al. (2011) for the metallicity of the SMC, Z=0.004. These models use a standard evolutionary code deriving outer boundary conditions from detailed atmospheric models that cover a large range of stellar metallicities, helium abundances, masses, and ages. They do not include stellar rotation, effects of magnetic fields, or accretion. We note that these omitted model parameters may result in overestimates of luminosity and therefore overestimates of stellar masses. The models cover a range of metallicities from Z=0.0002-0.03, stellar masses from $M=0.2-7.0\,M_\odot$, and ages from 1 to $100\,\mathrm{Myr}$.

When plotted on the HRD, our estimated temperatures and luminosities indicate that our HAeBe candidates are currently stars with spectral types F-B (source #9 is at the warm end of type G), are on intermediate-mass evolutionary tracks ranging from $3 M_{\odot}$ to $10 M_{\odot}$, and have ages less than 2 Myr (Table 3). Correction for additional extinction from circumstellar material would move our HAeBe candidates up and to the left in the HRD. Eight of our sources (#1, #4, #6, #7, #8, #9, SMC YSO 14, and SMC YSO 20) are more luminous than Galactic HAeBe stars with the same temperatures (as surveyed by Vioque et al. 2018, who used parallaxes and photometry from Gaia Data Release 2 to analyze 252 Galactic HAeBe stars). It is not surprising that our SMC HAeBe stars are systematically more luminous than their Galactic counterparts. Lamers et al. (1999), Beaulieu et al. (2001), and de Wit et al. (2003) reported that SMC sources, which they identified as possible HAeBe stars, were ~10 times more luminous than Galactic HAeBe stars of the same effective temperatures. They suggested that this could be due to higher accretion rates and/or lower dust abundance in the SMC HAeBe systems. We also observe that our candidate HAeBe stars are overluminous by roughly a factor of 10 so we may be observing one or both of these phenomena. Kamath et al. (2014) observed that their YSO candidates all appear to the right of the stellar birth line in the HRD, suggesting that PMS stars in the metal-poor environment of the SMC are less obscured and therefore observable at an earlier, more luminous stage of evolution. Our results are consistent with this conclusion.

3.2. Disk Properties from Optical and Infrared Spectra and Photometry

It is possible to determine disk properties from our measured spectra and SEDs if we assume that the strong infrared excess emission from our candidate HAeBe stars originates in protoplanetary disks. In principle optimal extraction, which gives higher weighting to higher S/N data, enhances the spatial resolution of the Spitzer IRS spectra for point sources and suppresses low-level extended emission filling the slits. While the optimal extraction improves the S/N of our spectra, it is still impossible to directly constrain the source of the MIR emission (Figure 5): projected widths of our spectrograph slits at the distance of the SMC range from 0.54 pc for the optical spectra to 3.2 pc for the longest wavelength IRS spectra. Thus we cannot directly constrain the origin of the infrared emission to a compact source (e.g., protoplanetary disk) or a more extended source (e.g., circumstellar envelope or surrounding ISM).

Target	3.6 μm (mag)	4.5 μ m (mag)	5.8 μm (mag)	$8.0~\mu \mathrm{m}$ (mag)	24 μm (mag)	$70~\mu\mathrm{m}$ (mJy)	100 μm (mJy)	160 μm (mJy)	$250~\mu \mathrm{m}$ (mJy)	350 μm (mJy)	500 μm (mJy)	Other ID
1	13.49 ± 0.07	12.65 ± 0.06	11.09 ± 0.04	9.73 ± 0.03	5.01 ± 0.05	588 ± 8	445 ± 37	222 ± 49	169 ± 13	22 ± 18		a
2	13.13 ± 0.02	12.2 ± 0.2	11.18 ± 0.04	9.32 ± 0.03	4.50 ± 0.02	900 ± 11	475 ± 42	525 ± 57	355 ± 17	274 ± 18	173 ± 16	Hodge 108
3	14.35 ± 0.06	14.1 ± 0.1	12.11 ± 0.02	10.6 ± 0.1	6.09 ± 0.5		259 ± 34					
4	13.34 ± 0.03	12.35 ± 0.02	11.24 ± 0.01	9.88 ± 0.04	3.67 ± 0.01	1031 ± 12	988 ± 59	831 ± 79	486 ± 24	369 ± 29	274 ± 27	WSHB 63
5	13.82 ± 0.01	13.7 ± 0.2	11.69 ± 0.06	10.21 ± 0.05	5.94 ± 0.06	219 ± 5	331 ± 30	387 ± 50	183 ± 15	121 ± 19		
6	14.08 ± 0.05	13.57 ± 0.09	12.05 ± 0.04	10.53 ± 0.04	6.20 ± 0.06							
7	14.6 ± 0.1	14.3 ± 0.1	12.39 ± 0.06	10.9 ± 0.2	7.11 ± 0.01	125 ± 2		134 ± 26	78 ± 5			
8	13.38 ± 0.08	12.83 ± 0.08	11.3 ± 0.1	9.49 ± 0.09	3.1 ± 0.3	1028 ± 11	834 ± 50	534 ± 51	175 ± 10	99 ± 10		LIN 238
9	13.22 ± 0.06	12.41 ± 0.08	11.57 ± 0.04	10.00 ± 0.05	5.84 ± 0.06		148 ± 37	211 ± 48	163 ± 13			a
10	13.1 ± 0.2	12.3 ± 0.1	11.18 ± 0.06	9.70 ± 0.07	5.10 ± 0.04	342 ± 5	485 ± 33	379 ± 41	169 ± 10	90 ± 12		a
SMC YSO 5	12.57 ± 0.07	11.51 ± 0.06	10.56 ± 0.03	8.87 ± 0.01	5.2 ± 0.04	221 ± 3	180 ± 24	216 ± 37	217 ± 10	213 ± 13	151 ± 13	ь
SMC YSO 14	12.9 ± 0.1	12.18 ± 0.03	10.91 ± 0.02	9.24 ± 0.05	4.5 ± 0.04	461 ± 6	492 ± 36	410 ± 46	227 ± 11	174 ± 14	89 ± 12	b,a
SMC YSO 20	12.6 ± 0.3	11.27 ± 0.07	10.41 ± 0.07	9.34 ± 0.05	4.8 ± 0.04	281 ± 6	383 ± 37	444 ± 60	387 ± 22	347 ± 27	•••	b

Notes. 3.6 and 4.5 μ m magnitudes are an average of WISE, NEOWISE, and SAGE-SMC (IRAC) data; 8 and 24 μ m magnitudes are from SAGE-SMC (IRAC and MIPS); 70–500 μ m flux densities are from the Herschel HERITAGE survey.

^a Sources identified by Kamath et al. (2014) as possible YSOs in their search for post-AGB/RGB candidates in the SMC.

b Sources identified by Oliveira et al. (2013) as possible HAeBe stars in their study of embedded YSOs in the SMC.

Table 3
Derived Stellar Characteristics

HAeBe Candidate	A_V^{a}	T_e (K)	L/L_{\odot}	M/M_{\odot}	Age (Myr)	Test Star	$T_e (K)^b$	$T_e (K)^c$
1	0.54	7500 ± 500	163	4	<1	HD 128801	10500	10000
2	0.45	10500 ± 500	115	3	1–2	HD 194453	9520	10000
3	0.66	13000 ± 1000	2447	7	<1	HD 164257	9520	9000
4	0.50	6500 ± 500	236	4–5	<1	HD 147550	10500	9000
5	0.50	9000 ± 500	433	5	<1	HD 16031	7200	6750
6	0.66	8500 ± 500	1011	7	<1	HD 167278	6440	6000
7	0.56	6750 ± 500	466	5–6	<1	HD 205202	6440	6000
8	0.50	8500 ± 500	1516	6–7	<1	HD 175805	6280	6000
9	0.53	6000 ± 500	276	5	<1	HD 161770	6740	6250
10	0.53	21000 ± 2000	3807	7	<1	HD 19019	6030	6250
SMC YSO 5	0.54	20000 ± 2000	7389	7–10	<1	HD 200081	5250	5500
SMC YSO 14	0.50	7250 ± 500	620	6	<1	HD 345957	6030	6250
SMC YSO 20	0.58	7000 ± 500	674	6	<1	HD 13043	5860	5750
•••	•••	•••	•••	•••	•••	HD 57060	38000	27000

Notes

^c Estimates using our continuum fitting method.

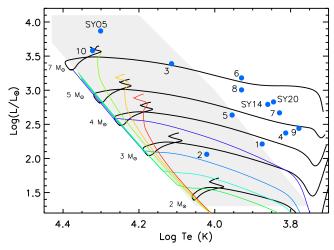


Figure 6. HRD showing our program stars (filled circles) plotted with model pre-main-sequence and main-sequence evolutionary tracks (black) for 3, 4, 5, and $7 \, M_{\odot}$) and isochrones for 1 (violet), 2, 3, 4, 35, 65, and 100 Myr (red). Models are from Tognelli et al. (2011) and assume SMC metallicity of Z=0.004. Gray shading indicates the region occupied by most Galactic HAeBe stars (Vioque et al. 2018).

Our disk candidates all have strong infrared excesses longward of $\lambda \sim 1~\mu m$; all have relatively high-contrast PAH emission; all have continuum emission from silicate dust, and one source (#4) has $10~\mu m$ silicate absorption; all have emission features from gas (notably H₂); nine show signs of a blue-continuum excess; and two sources (#4 and SMC YSO 5) have a solid-state CO₂ absorption feature at 15 μm .

3.2.1. Spectral Energy Distributions

We have compiled SEDs for each of our candidate HAeBe sources (Figure 7). We present these data for each source plotted with the Castelli and Kurucz stellar photosphere (black trace) that best fits the optical spectra (the same models used to estimate photospheric temperatures and presented in Figure 3). All of the SEDs resemble the Lada Class II accreting disk phase, with several sources (3, 6, 7, 8, and SMC YSO 5)

Table 4 $H\alpha$ Emission Properties

Target	$\lambda_{\mathrm{H}\alpha}$ (Å)	FWHM _{Hα} (Å)	$\text{FW}10\%_{\text{H}lpha}(\mathring{\text{A}})$	Blue Excess ^a
1	6564.1	6.0	11.3	✓
2	6566.2	7.6	15.9	✓
3	6563.2	8.3	13.1	✓
4	6566.2	7.4	13.1	✓
5	6564.6	9.1	17.1	✓
6	6563.3	8.9	18.5	✓
7	6565.4	7.2	16.5	
8	6564.0	8.6	20.6	✓
9	6567.0	9.0	19.6	✓
10	6564.5	5.0		
SMC YSO 5	6565.2	3.0		
SMC YSO 14	6564.8	9.6	16.8	✓
SMC YSO 20	6562.9	9.2	18.8	

Note.

showing a dip in NIR-continuum emission (as measured by the NIR photometry), resembling pretransition disks. The mid- and far-IR show a turnover intensity in the range $\lambda=30\text{--}70~\mu\text{m}$ for all 13 sources. All of the candidate HAeBe stars have strong NIR and MIR excesses, which implies early stages of disk evolution and also suggests that they should exhibit strong indicators of disk–star accretion, the subject of the next section.

3.2.2. Ha Emission and Blue Continuum Excess

Optical emission in the hydrogen recombination lines, primarily $H\alpha$, is an indicator of disk-star mass accretion in protoplanetary disk systems. Hydrogen recombination emission is also common in PNe, H II regions, and Classical Be (CBe) stars, but in these sources all of the Balmer lines tend to be strongly in emission, while in the protoplanetary disks of intermediate-mass stars $H\alpha$ emission tends to dominate, and this is indeed the case for our targets. Line widths enable us to

^a A_V from Rubele et al. (2018) used for reddening correction applied to our optical spectra and UBVIJHK_s photometry.

^b Estimates from Chen et al. (2014).

 $[^]a$ Excess emission on the blue side of the Balmer jump ($\lambda < 4~\mu m)$ observed in optical spectra (Figure 3).

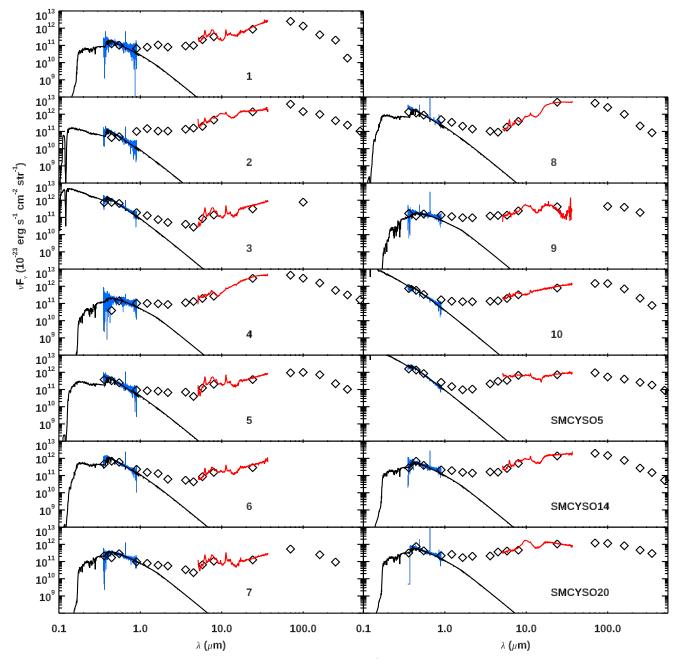


Figure 7. Spectral energy distributions of our candidate HAeBe sources: 3800–9000 Å spectroscopy (blue trace, corrected for reddening); photometry (open diamonds, optical–NIR corrected for reddening); and 5–40 μ m spectra (red trace, *Spitzer* IRS). We present these data plotted for each of our sources with the Kurucz stellar photosphere that best fits the optical spectra (black trace).

distinguish $H\alpha$ emission in various astrophysical contexts and Table 4 summarizes the measured $H\alpha$ properties for our candidate HAeBe stars. Since all of our candidate HAeBe stars have strong emission from dust, it is unlikely that they are CBe stars, which have IR excesses from bound–free and free–free emission in very warm gas-rich, non-planet-forming, excretion disks.

The $H\alpha$ emission lines in our sample have a mean FWHM of ${\sim}300~{\rm km\,s^{-1}}$ and are single-peaked. With a resolution of $174~{\rm km\,s^{-1}}$ in our spectra it would be difficult to resolve double-peaked line profiles. If they are single-peaked, the widths of the $H\alpha$ lines for our candidate HAeBe stars may indicate high rotation rates of material close to the stars, e.g., accretion flows.

Nine of our candidate HAeBe stars (1–6, 8, 9, and SMC YSO 14) have veiling (excess emission) on the blue side of the Balmer jump. Blue and near-UV excesses and far-UV line emission from Ly α -pumped H₂ are common features in the spectra of Galactic protoplanetary disk systems in the accretion phase of their evolution (France et al. 2011; Ingleby et al. 2011; Cauley & Johns-Krull 2016). A blue–UV excess correlates strongly with other indicators of gas accretion, like H α and Br γ emission, in protoplanetary disks (Garrison 1978; Muzerolle et al. 2004; Donehew & Brittain 2011). Sources 1–9, SMC YSO 14, and SMC YSO 20 have H α emission, which leaves only #10 and SMC YSO 20 without any observed accretion signature. These two sources are the most evolved in our sample, both lying close to the zero-age main sequence in

 0.17 ± 0.04

					<i>-</i>			
Target	6.2 (μm)	$F_{6.2}$ (10 ⁻¹⁶ Wm ⁻²)	7.7–8.2 μm (μm)	$F_{7.7-8.2}$ (10 ⁻¹⁶ Wm ⁻²)	11.3 μm (μm)	$F_{11.3}$ (10 ⁻¹⁶ Wm ⁻²)	12.7 μm (μm)	$F_{12.7}$ (10 ⁻¹⁶ Wm ⁻²)
1	6.22 ± 0.01	1.62 ± 0.10	7.78 ± 0.04	4.80 ± 0.17	11.28 ± 0.01	1.23 ± 0.03	12.70 ± 0.06	0.32 ± 0.04
2	6.22 ± 0.02	1.00 ± 0.08	7.68 ± 0.07	1.48 ± 0.12	11.29 ± 0.02	0.95 ± 0.06	12.66 ± 0.2	0.19 ± 0.04
3	6.22 ± 0.02	0.94 ± 0.09	7.83 ± 0.03	2.56 ± 0.08	11.29 ± 0.01	0.87 ± 0.03	12.70 ± 0.05	0.14 ± 0.02
4	6.21 ± 0.05	0.35 ± 0.06	7.75 ± 0.09	2.34 ± 0.20	11.29 ± 0.02	0.33 ± 0.03	12.3 ± 0.2	0.07 ± 0.02
5	6.22 ± 0.01	1.31 ± 0.07	7.72 ± 0.03	1.89 ± 0.07	11.29 ± 0.01	1.27 ± 0.03	12.72 ± 0.04	0.23 ± 0.02
6	6.20 ± 0.02	0.52 ± 0.05	7.75 ± 0.07	0.81 ± 0.08	11.29 ± 0.01	0.60 ± 0.02	12.8 ± 0.2	0.11 ± 0.04
7	6.22 ± 0.05	0.58 ± 0.12	7.81 ± 0.04	1.43 ± 0.06	11.29 ± 0.01	0.54 ± 0.02	12.7 ± 0.2	0.09 ± 0.02
8	6.20 ± 0.01	1.05 ± 0.05	7.69 ± 0.03	1.32 ± 0.06	11.30 ± 0.01	0.85 ± 0.02	12.76 ± 0.04	0.12 ± 0.02
9	6.17 ± 0.20	0.15 ± 0.08	8 ± 1	0.14 ± 0.11	11.29 ± 0.05	0.27 ± 0.05	12.76 ± 0.03	0.25 ± 0.02
10	6.20 ± 0.05	0.65 ± 0.12	7.74 ± 0.08	0.94 ± 0.09	11.29 ± 0.04	0.59 ± 0.07	12.7 ± 0.3	0.12 ± 0.05
SMC YSO 5	6.21 ± 0.05	0.39 ± 0.06	7.9 ± 0.1	1.68 ± 0.11	11.31 ± 0.03	0.48 ± 0.04	12.5 ± 0.4	
SMC YSO 14	6.22 ± 0.06	1.52 ± 0.38	7.71 ± 0.05	2.68 ± 0.17	11.29 ± 0.01	1.24 ± 0.06	12.67 ± 0.03	0.24 ± 0.02

 0.68 ± 0.52

 11.29 ± 0.03

Table 5
PAH Feature Center Wavelengths and Integrated Feature Strengths

Figure 6, so we should expect them to show weak or absent accretion. This result is also consistent with the suggestion that accretion may be partly responsible for the increased luminosity of the SMC HAeBe stars relative to Galactic HAeBe stars (Section 3.1).

 0.48 ± 0.09

 7.8 ± 0.8

 6.22 ± 0.06

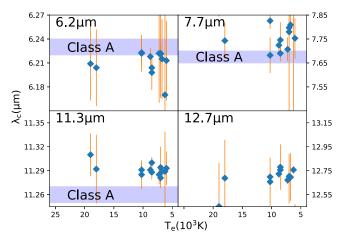
SMC YSO 20

3.2.3. PAH Emission

Since the PAH features were first observed in H II regions, the wavelengths of PAH features as seen in the ISM are commonly listed: $6.2 \, \mu m$, a complex of features at 7.7, 8.6, 11.3, and 12.7 μm , and a complex of features at 17.0 μm . We have fitted and removed the $5{\text -}13 \, \mu m$ continuum in our IRS spectra, isolated and extracted the strongest PAH features $(6.2{\text -}12.7 \, \mu m)$, and then measured their central wavelengths and integrated fluxes (Table 5). We used a cubic spline to fit and subtract the continuum using anchor points between the PAH features. This method of isolating the PAH features for further quantitative analysis is described in detail by Sloan et al. (2007) and by K08. The method avoids the use of mineralogical modeling, and makes no assumptions about mineralogy, in order to fit and remove the dust continuum and (when present) solid-state features.

Following Peeters et al. (2002) and Sloan et al. (2007) we adopt a classification scheme of PAH spectra based on the wavelengths of emission features: Class A PAHs (features at 6.20, 7.65, and 11.25 μ m), Class B PAHs (features shifted to 6.30 and 7.85 μ m), and Class C PAHs (peak of the 7.65–7.85 μ m complex shifted to the red side of 8.0 μ m and 11.25 μ m feature shifted to ~11.4 μ m). Sloan et al. (2007) and K08 interpreted these shifts as indicators of PAH processing by stellar radiation, with Class C indicating minimal photoprocessing and Class A indicating more photoprocessing.

The PAH emission in our SMC sample are generally consistent with Class A, showing little or no variation of PAH feature central wavelengths with $T_{\rm e}$ (Figure 8) and therefore implying that they are more photoprocessed as observed in the ISM, e.g., in reflection nebulae or in H II regions near young, high-mass stars. If these are isolated HAeBe stars, then this characteristic distinguishes them from Galactic HAeBe stars, which generally fall between Class B and C and show a linear decrease of feature wavelengths with increasing stellar $T_{\rm e}$ (Sloan et al. 2005 and K08). We note again, however, that none of our sources is deeply embedded



 0.65 ± 0.06

 12.7 ± 0.2

Figure 8. Our observed wavelengths of the 6.2, 7.7, 11.3, and 12.7 μ m PAH features compared to stellar effective temperatures for our candidate HAeBe stars. Wavelength ranges for Class A PAH features are indicated with shaded regions. Wavelengths for Class B and C PAH spectra fall above the maximum vertical scale in all panels.

within optical nebulosity and our estimated luminosities and photospheric temperatures indicate intermediate mass, so the sources of the PAH emission may not be in a strongly ionizing external (interstellar) radiation field. It may be that the PAH emission originates in general nebulosity from a reflection nebula in the beams of our infrared observations, but the emission could also come from protoplanetary disk systems with PAHs excited to emission by radiation from their host stars. Adams et al. (2013) observed 20 dusty OB stars in the SMC in search of debris disks. They concluded that the strong 24 μ m point sources are not debris disks, but may be cirrus hot spots or possibly high-mass analogs to transition disks. Observations with the spatial resolution necessary to directly and definitively identify the source of the infrared excess in SMC candidate YSOs and HAeBe stars do not vet exist.

If radiation from the host stars is illuminating PAHs located in circumstellar disks, then this circumstellar material may be systematically more photoprocessed in the relatively dust-poor SMC compared to their Galactic counterparts. In this case the host stars themselves could be ionizing and breaking up PAHs

Tab	le 6
Mid-infrared Spect	ral Line Detections

Target	Silicate	$\rm H_2$ 6.91 $\mu \rm m$	$\rm H_2$ 9.67 $\mu \rm m$	$\rm H_2~12.28~\mu m$	$\rm H_2$ 17.03 $\mu \rm m$	CO_2	[Ne II]	[S III]
1	X	√?	✓	✓	✓	X	✓	X
2	✓	✓	√ ?	✓	✓	√ ?	X	X
3	X	X	✓	✓	✓	X	✓	X
4	✓	✓	✓	✓	✓	✓	X	X
5	X	X	✓	✓	X	X	✓	X
6	X	✓	✓	X	✓	X	✓	X
7	X	✓	✓	✓	✓	X	✓	X
8	√ ?	✓	✓	✓	✓	X	✓	X
9	✓	X	√ ?	✓	✓	X	✓	✓
10	√ ?	✓	✓	✓	X	X	✓	X
SMC YSO 5	√ ?	✓	✓	✓	X	X	✓	X
SMC YSO 14	√ ?	✓	✓	✓	X	X	✓	X
SMC YSO 20	√ ?	✓	✓	✓	X	X	✓	X

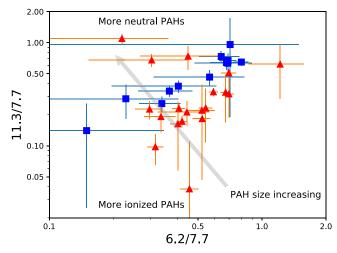


Figure 9. Ratios of the PAH-feature strengths for our candidate HAeBe stars (blue squares): $11.3 \ \mu m/7.7 \ \mu m$ vs. $6.2 \ \mu m/7.7 \ \mu m$. For comparison we also plot a sample of Galactic HAeBe stars (red triangles, data from K08 Table 4). PAH ionization increases from top to bottom. PAH molecule size (number of carbon atoms) increases from lower right to upper left (arrow).

on the surfaces of their own circumstellar disks. The 6.2 and 7.7 μ m features originate in C–C bonds (Allamandola et al. 1985) and these features are enhanced in ionized PAHs. The 11.3 μ m feature, originating from the C-H bending mode, is enhanced in neutral PAHs (Allamandola et al. 1999; Draine 2003; Draine & Li 2007; Sandstrom et al. 2012). Therefore, $F_{11.3}/F_{7.7}$ decreases as the degree of PAH ionization increases. We present a plot of $F_{11,3}/F_{7,7}$ versus $F_{6,2}/F_{7,7}$ in Figure 9. Neutral PAH emission will tend to fall toward the upper region in this plot and ionized emission toward the lower region. Our SMC observations fall on a distribution from lower left to upper right in Figure 9 indicating a range of ionization, but a smaller range of PAH sizes. We include a sample of Galactic HAeBe stars (K08) in Figure 9 for comparison. Galactic HAeBe stars host PAHs with increasing ionization as the PAHs get smaller, an effect attributed to photoprocessing (K08). Our candidate HAeBe stars span a range indicating a continuum from ionized to neutral PAHs. The diversity of PAH ionization in the SMC indicates that the degree of photoprocessing in SMC HAeBe disks may be more diverse than the "A" PAH classification implies (Figure 8). The Galactic HAeBe stars span a much larger range of PAH sizes, indicated by the larger scatter from lower right to upper left in Figure 9, than the SMC HAeBe candidates we observed.

The relationships we have identified between the PAH features may be explained by differences in the structures of the inner disks and/or the degree of radial flaring in the outer disks. In systems where the inner disks are cleared or partially cleared of gas and dust (presumably by the formation of planets) the photospheric radiation may be less attenuated and shielded and so illuminate more of the material in the surface of the inner disk wall and/or on the surface of a radially flared disk. A radially flared disk would present even more area to the central star for photoprocessing. K08 suggested both possibilities for Galactic HAeBe stars based on detailed analysis of the mid-IR SEDs and modeling of HAeBe disk evolution. If the infrared emission we observe is optically thick (e.g., from a disk), then the inclination angles at which we have observed our candidate HAeBe star disks may also play a role in the diversity of PAH spectra that we have measured. The range of PAH ionization that we observe could indicate the presence of highly photoprocessed, ionized PAHs located in an inner disk cleared of dust and less photoprocessed, more neutral PAHs located in the outer disk.

3.2.4. Molecular Hydrogen Emission

Emission from pure rotational transitions of molecular hydrogen is present in the infrared spectra for all of our 13 candidate HAeBe (Table 6). The H₂ emission features at 6.91, 9.67, 12.28, and 17.03 μ m, which correspond to the S(5), S(3), S(2), and S(1) transitions, respectively, have been difficult to detect in Galactic protoplanetary disk sources. The Spitzer HAeBe spectra presented in K08 do not show H₂ emission features, but van den Ancker et al. (2000) detected H₂ pure rotational emission toward two Galactic HAeBe stars, and Thi et al. (2001) reported detections of the S(0) and S(1) transition lines in Galactic T Tauri and HAeBe stars. Bitner et al. (2007) later detected the S(1), S(2), and S(4) transition lines in AB Aur while Martin-Zaïdi et al. (2010) detected the S(1) transition in the HAeBe stars HD 97048 and AB Aur. More recently Oliveira et al. (2013) detected and analyzed pure rotational emission in a sample of high-mass YSOs in the SMC.

We have estimated H_2 column densities from emission line fluxes and then estimated rotational temperatures by generating excitation diagrams (Figure 10) using the same method as Oliveira et al. (2013). We calculate the column density of

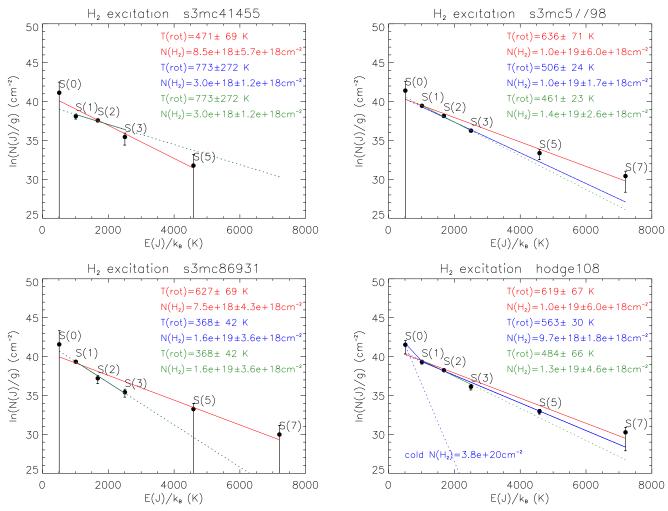


Figure 10. Excitation diagrams for emission from H_2 pure rotational emission from selected sources in our HAeBe candidate sample. Slopes of linear fits to the data yield gas temperature estimates: red lines fit all detections; blue lines fit only points with N_J /error > 1; green lines fit only S(1), S(2), and S(3); dotted blue line S(0) is used to estimate contributions from a cold component with T = 100 K.

molecules in the upper J energy state

$$N_J = \frac{F_J}{\Delta E_J h c A_J},\tag{1}$$

where F_J is the line flux in erg s⁻¹ cm⁻², ΔE is the transition energy in wave numbers, and A_J is the Einstein A coefficient in s⁻¹. We plot $\frac{N_J}{g_J}$ (where $g_J = g_s(2J+1)$ is statistical weight) as a function of the energy of the corresponding J state (E_J/k) in kelvins). We have estimated the H₂ rotational temperature from the slope of the resulting excitation diagram assuming local thermodynamic equilibrium (LTE):

$$\ln\left(\frac{N_J}{g_J}\right) = -\frac{E_J}{kT}.$$
(2)

In calculating statistical weights we assume g_s , the nuclear spin statistical weight, has the ortho–para ratio equilibrium value of $g_s = 3$.

Our estimated H₂ column densities fall in the range, $N_{\rm H_2} = 2.5 \pm 0.7 \times 10^{18} \, \rm cm^{-2}$ to $N_{\rm H_2} = 1.6 \pm 0.4 \times 10^{19} \, \rm cm^{-2}$, and the corresponding rotational temperatures cover the range, $T = 368 \, \rm K \pm 42 \, K$ to $T = 910 \, \rm K \pm 97 \, K$. Column densities estimated

solely from the S(0) feature for our candidate HAeBe stars are systematically higher than the LTE fit to the other transitions, as found by Oliveira et al. (2013), suggesting that there is a reservoir of cold quiescent gas in these sources in addition to the warm component. Fits to these estimates are linear, which indicates LTE and therefore predominantly thermal excitation. The fact that our $\frac{N_J}{g_J}$ values fall along a linear distribution shows that our assumption of $g_s=3$ is appropriate; this equilibrium value of the statistical weight is also consistent with our assumption of LTE for the H₂ emission.

Carmona et al. (2008) suggest that the pure rotational lines from $\rm H_2$ are more likely to be detected if the gas-to-dust ratio is high and/or the gas-to-dust temperature ratio is high, with the latter ratio having a larger impact. They come to this conclusion by adjusting the two-layer disk model presented by Dullemond et al. (2001) to account for differences in gas-to-dust ratios and gas-to-dust temperature ratios. We expect the gas-to-dust ratio to be higher in metal-poor disk sources in the SMC relative to their Galactic counterparts, which may lead to a higher gas-to-dust temperature ratio. This can explain the strong rotational emission from molecular hydrogen in our sample relative to Galactic HAeBe stars.

Continuing to explore the possibility that the infrared emission we observe is from circumstellar disks: the PAH and H₂ emission may indicate a fundamental difference between HAeBe stars in the SMC and Milky Way galaxies. We suggest that in the SMC emission from HAeBe stars is characterized by PAH emission from more highly photoprocessed PAHs (as observed in the photon-dominated regions of Galactic starforming nebulae) and H₂ emission from gas that is warmer relative to the dust. In the more metal-poor SMC, reduced shielding of stellar radiation by dust may result in stronger irradiation with a deeper radial extent into the inner disk walls and outer disk surfaces. van Loon et al. (2010) proposed that the lower dust/gas ratio in the more metal-poor SMC reduces the cooling efficiency (due to lower abundance of oxygen, molecules, and dust), which results in warmer dust farther out in the disks. Similarly, Ward et al. (2017) have observed a lower fraction of CO bandhead emission in higher-mass SMC YSOs relative to the Milky Way, which they suggest may indicate higher temperatures and more CO destruction due to less shielding from dust relative to disks in the Milky Way.

3.2.5. Possible Multiplicity of Sources

In their study of dusty OB stars in the SMC, Adams et al. (2013) noted that the low spatial resolution of MIR observations complicates the full characterization of objects in the SMC. Oliveira et al. (2013) and Ward et al. (2017) observed multiplicity of YSOs in the SMC using adaptive optics to obtain high angular resolution NIR images. More recently, Stephens et al. (2017) demonstrated the utility of high spatialresolution imaging in exploring the multiplicity of sources in the Magellanic Clouds with their Hubble Space Telescope (HST) investigation of OB associations in the Large Magellanic Cloud. Our interpretation of optical spectra and infrared excess emission from our candidate HAeBe stars depends on the assumption that we are observing material in circumstellar disks rather than the surrounding ISM, but the highest spatial resolution we achieved in the present study is 1"8, which translates to 0.54 pc (109,320 au) at $d_{SMC} = 61.7$ kpc. Typical Galactic protoplanetary disks have radii of several tens to several hundreds of astronomical units so the detailed spatial nature of the emission we have observed is unknown. It is possible that emission in the different observational wavebands comprising our SEDs originates in protoplanetary disks, but it is also possible that the emission is from different regions separated by much more than the typical size scales of protoplanetary disks. Acquisition of high spatial-resolution imaging (e.g., using HST, ground-based NIR imaging using adaptive optics, NIR and MIR using the James Webb Space Telescope, and submillimeter/millimeter using the Atacama Large Millimeter Array) will enable exploration into the spatial extent of emission across the SEDs for these sources.

We are currently analyzing archival *UV* and visible images of two of our sources (#3 and SMC YSO 20), taken with the *HST* Wide-Field Camera and Wide-Field Planetary Camera (serendipitous observations in a unrelated study: HST Proposal ID 13659; Sandstrom 2014). These images show that SMC YSO 20 is a single point source, but source #3 is a tight cluster of nine bright optical point sources—free of optical nebulosity —within a 1.18 circular region centered on our target coordinates (T. Knapp et al. 2019, in preparation). The image has spatial resolution of 0.108 projecting to a size of 4900 au at the SMC distance, much closer to the size of a protoplanetary

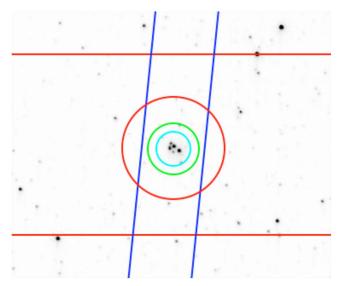


Figure 11. *R*-band image of one of our candidate HAeBe stars (#3), taken with the *Hubble Space Telescope* Wide-Field Camera 3 (resolution FWHM = 0.008). We indicate characteristic widths of the point-spread functions of our spectroscopic and photometric observations: optical spectra (cyan, smallest circle 1.008), 2MASS NIR photometry (green, larger circle, 2.008), MIPS $24 \mu m$ photometry (red, largest circle, 608), *Spitzer* IRS Short-Low slit width (nearly vertical blue parallel lines, 3.008, and Long-Low slit width (horizontal red parallel lines, 10.008).

disk (Figure 11). Source #3 is the third hottest and most luminous of our candidates and has PAH emission indicating a higher degree of photoprocessing relative to the others in our sample. None of these characteristics distinguishes source #3 from the others without the benefit of high spatial resolution. Thus it appears that at least one of our sources consists of multiple components that are unresolved in our spectroscopic and photometric observations. Since there is no bright nebulosity in this image, we assume that material within \sim 2500 au of one (or perhaps more than one) of these objects is responsible for the NIR, MIR, and FIR emission that we observe in source #3.

4. Summary and Future Work

We have identified 13 sources that appear to be intermediatemass PMS stars (HAeBe stars) in the SMC, initially selected from NIR and MIR colors and then followed up with optical and infrared spectroscopy. We have derived the following characteristics for our sample of candidate HAeBe stars:

- 1. None of the candidate HAeBe stars have yet been identified as embedded YSOs, post-asymptotic giant branch stars, planetary nebulae, compact H II regions, or Classical Be stars.
- 2. All but one of the candidates (Figure 11) are point sources in observations spanning optical–far-infrared that are isolated from, but often near, regions of strong nebular emission. We directly observed the stellar photospheres, so we conclude that these are not embedded YSOs. The sample consists of PMS stars (types F–B, with one early type G) in the 3–10 M_{\odot} range with ages less than 2 Myr.
- 3. The infrared excesses in all sources are strongly reminiscent of Galactic Herbig Ae/Be stars. IR spectra of some sources show silicate emission (in one case absorption) and pure-rotational H_2 emission. The source

with silicate dust absorption also has CO_2 ice absorption. This may be a star surrounded by cool material in an envelope or in the local ISM, but it is difficult to reconcile the relatively low line-of-sight extinction and lack of strong nebular emission toward all of our sources with strong obscuration by surrounding material.

- 4. Optical spectra show strong Balmer emission and excess blue-continuum emission. Both properties indicate active accretion disks in Galactic HAeBe stars. The excess emission that we observe at blue and near-UV wavelengths may indicate strong gas accretion onto the stellar photospheres. This property is consistent with a Class II stage of protoplanetary disk evolution especially when combined with the shapes of the SEDs, which strongly resemble those of Galactic HAeBe stars.
- 5. The candidates have systematically higher luminosities relative to Galactic HAeBe stars. This may be due to the higher accretion activity, and/or lower circumstellar extinction by dust in the metal-poor environment of the SMC. Lower circumstellar extinction may be allowing us to observe these systems at earlier, more luminous stages of PMS evolution.
- 6. All candidates show PAH emission in the mid-IR, which is characteristic of ~50% of Galactic HAeBe and ~6% of Galactic T Tau stars. However, a detailed analysis of PAH feature strengths and central wavelengths indicates that this emission is from highly photoprocessed PAHs like those in Galactic H II regions and reflection nebulae and span a range from more neutral to more ionized PAHs. The spatial resolution of our observations cannot directly distinguish PAH emission originating in a protoplanetary disk from more extended PAH emission originating in the immediately surrounding ISM.
- 7. Strong H₂ emission may indicate a high gas-to-dust ratio and/or a high ratio of gas temperature to dust temperature, which is consistent with strong inner protoplanetary disk irradiation by their host stars in the metal-poor environment of the SMC.
- 8. One of our candidate HAeBe stars (#3) is a tight cluster of optical point sources in archival *HST* images taken with 0.00% spatial resolution. There is no bright nebulosity between or immediately surrounding the cluster components. None of the observations leading to the SED presented in this paper were able to resolve this source into multiple components, so the precise origin of the infrared excess emission within the cluster is currently unknown.

A definitive identification of the source of infrared excess emission, distinguishing protoplanetary disks from circumstellar envelopes, will require future follow-up observations including NIR spectroscopy of our candidate HAeBe stars in search of gas emission and signatures of disk activity. For example, $Br\gamma$ line strengths, if present, can yield estimates of gas accretion rates that may correlate with the $H\alpha$ widths (Najita et al. 1996; Garcia Lopez et al. 2006; Kraus et al. 2008) and blue-UV excess. Br γ emission may also indicate the existence of protostellar winds. Br γ line profile shapes can aid us in determining gas dynamics (e.g., whether the ionized gas is in-falling or out-flowing, and whether the molecular gas is orbiting the stars in a disk). H₂ emission in the near-infrared rovibrational transitions traces warm gas in T Tau disk systems. Our observations of strong rotational H₂ emission, are consistent with origins in warm, gas-rich disks, which we

expect to also have strong rovibrational H_2 emission allowing us to determine basic physical characteristics of the warm molecular gas in the inner planet-forming disks: e.g., orbital dynamics, radial temperature, and density profiles in the gas disks, and disk radial structure. A program of high spatial resolution observations to explore of the precise origin of infrared excess emission from candidate protoplanetary disks in the SMC is also necessary.

L.K. is grateful to Ithaca College for resources in support of this work. We thank V. Gugliada for contributions to data analysis and an anonymous reviewer for suggestions and comments that significantly improved this paper. G.C.S. was supported by NASA through Contract Number 1257184 issued by the Jet Propulsion Laboratory, California Institute of Technology under NASA contract 1407, which funded GTO observations made with the Spitzer Space Telescope. We used observations made with the NASA/ESA Hubble Space Telescope, obtained from the data archive at the Space Telescope Science Institute under NASA contract NAS 5-26555, and observations made with Herschel, a European Space Agency Cornerstone Mission with significant participation by NASA. This research has made use of the SIMBAD database operated at the Centre de Données astronomiques de Strasbourg, the NASA Astronomical Data System (ADS), and the The Digitized Sky Survey, which was produced at the Space Telescope Science Institute under U.S. Government grant NAG W-2166.

ORCID iDs

Luke D. Keller https://orcid.org/0000-0003-1046-512X Joana M. Oliveira https://orcid.org/0000-0002-0861-7094 Kathleen E. Kraemer https://orcid.org/0000-0002-2626-7155

Jacco Th. van Loon https://orcid.org/0000-0002-1272-3017 A. A. Zijlstra https://orcid.org/0000-0002-3171-5469

References

```
Acke, B., & van den Ancker, M. E. 2004, A&A, 426, 151
Adams, J. J., Simon, J. D., Bolatto, A. D., et al. 2013, ApJ, 771, 112
Allamandola, L. J., Hudgins, D. M., & Sandford, S. A. 1999, ApJL, 511, L115
Allamandola, L. J., Tielens, A. G. G. M., & Barker, J. R. 1985, ApJL, 290, L25
Beaulieu, J.-P., de Wit, W. J., Lamers, H. J. G. L. M., et al. 2001, A&A,
   380, 168
Beintema, D. A., van den Ancker, M. E., Molster, F. J., et al. 1996, A&A,
  315, L369
Bernard-Salas, J., Peeters, E., Sloan, G. C., et al. 2009, ApJ, 699, 1541
Bernasconi, P. A. 1996, A&AS, 120, 57
Berthoud, M. G., Keller, L. D., Herter, T. L., Richter, M. J., & Whelan, D. G.
   2007, ApJ, 660, 461
Bibo, E. A., & The, P. S. 1991, A&AS, 89, 319
Bitner, M. A., Richter, M. J., Lacy, J. H., et al. 2007, ApJL, 661, L69
Boehm, T., & Catala, C. 1995, A&A, 301, 155
Bolatto, A. D., Simon, J. D., Stanimirović, S., et al. 2007, ApJ, 655, 212
Brittain, S. D., Simon, T., Najita, J. R., & Rettig, T. W. 2007, ApJ, 659, 685
Carlson, L. R., Sewiło, M., Meixner, M., et al. 2012, A&A, 542, A66
Carmona, A., van den Ancker, M. E., Henning, T., et al. 2008, A&A, 477, 839
Castelli, F., & Kurucz, R. L. 2003, in IAU Symp. 210, Modelling of Stellar
   Atmospheres, ed. N. Piskunov, W. W. Weiss, & D. F. Gray (San Francisco,
   CA: ASP), A20
Cauley, P. W., & Johns-Krull, C. M. 2016, ApJ, 825, 147
Chen, Y.-P., Trager, S. C., Peletier, R. F., et al. 2014, A&A, 565, A117
Cioni, M.-R. L., Clementini, G., Girardi, L., et al. 2011, A&A, 527, A116
Cioni, M.-R., Loup, C., Habing, H. J., et al. 2000, A&AS, 144, 235
Cutri, R. M., Skrutskie, M. F., van Dyk, S., et al. 2003, The IRSA 2MASS All-
```

Sky Point Source Catalog, NASA/IPAC Infrared Science Archive, http://

irsa.ipac.caltech.edu/applications/Gator/

```
de Wit, W. J., Beaulieu, J.-P., Lamers, H. J. G. L. M., Lesquoy, E., &
  Marquette, J.-B. 2003, A&A, 410, 199
Dominik, C., Dullemond, C. P., Waters, L. B. F. M., & Walch, S. 2003, A&A,
  398, 607
Donehew, B., & Brittain, S. 2011, AJ, 141, 46
Draine, B. T. 2003, ARA&A, 41, 241
Draine, B. T., & Li, A. 2007, ApJ, 657, 810
Dullemond, C. P. 2002, A&A, 395, 853
Dullemond, C. P., Dominik, C., & Natta, A. 2001, ApJ, 560, 957
Dullemond, C. P., Henning, T., Visser, R., et al. 2007, A&A, 473, 457
Dullemond, C. P, & Dominik, C. 2004, A&A, 417, 159
Ercolano, B., & Clarke, C. J. 2010, MNRAS, 402, 2735
Fabregat, J., & Torrejón, J. M. 2000, A&A, 357, 451
Fairlamb, J. R., Oudmaijer, R. D., Mendigutía, I., Ilee, J. D., &
   van den Ancker, M. E. 2015, MNRAS, 453, 976
Fitzpatrick, Massa 1999, PASP, 111, 6
France, K., Yang, H., & Linsky, J. L. 2011, ApJ, 729, 7
Furlan, E., Hartmann, L., Calvet, N., et al. 2006, ApJS, 165, 568
Garcia Lopez, R., Natta, A., Testi, L., & Habart, E. 2006, A&A, 459, 837 Garrison, L. M., Jr. 1978, ApJ, 224, 535
Gatley, I., Hyland, A. R., & Jones, T. J. 1982, MNRAS, 200, 521
Ghez, A. M., McCarthy, D. W., Patience, J. L., & Beck, T. L. 1997, ApJ,
  481, 378
Gordon, K. D., Meixner, M., Meade, M. R., et al. 2011, AJ, 142, 102
Graczyk, D., Pietrzyński, G., Thompson, I. B., et al. 2014, ApJ, 780, 59
Hajduk, M., Gładkowski, M., Soszyński, I., et al. 2014, A&A, 561, A8
Hamidouche, M., Wang, S., & Looney, L. W. 2008, AJ, 135, 1474
Herbig, G. H. 1960, ApJS, 4, 337
Hernández, J., Briceño, C., Calvet, N., et al. 2006, ApJ, 652, 472
Hernández, J., Calvet, N., Briceño, C., Hartmann, L., & Berlind, P. 2004, AJ,
   127, 1682
Hernández, J., Calvet, N., Hartmann, L., et al. 2005, AJ, 129, 856
Houck, J. R., Roellig, T. L., van Cleve, J., et al. 2004, ApJS, 154, 18
Ingleby, L., Calvet, N., Bergin, E., et al. 2011, ApJ, 743, 105
Jameson, K. E., Bolatto, A. D., Leroy, A. K., et al. 2016, ApJ, 825, 12
Kamath, D., Wood, P. R., & Van Winckel, H. 2014, MNRAS, 439, 2211
Kato, D., Nagashima, C., Nagayama, T., et al. 2007, PASJ, 59, 615
Keller, L. D., Sloan, G. C., Forrest, W. J., et al. 2008, ApJ, 684, 411
Kemper, F., Woods, P. M., Antoniou, V., et al. 2010, PASP, 122, 683
Kenyon, S. J., & Hartmann, L. 1995, ApJS, 101, 117
Kraemer, K. E., Sloan, G. C., Bernard-Salas, J., et al. 2006, ApJL, 652, L25
Kraemer, K. E., Sloan, G. C., Wood, P. R., Jones, O. C., & Egan, M. P. 2017,
   ApJ, 834, 185
Kraus, S., Hofmann, K.-H., Benisty, M., et al. 2008, A&A, 489, 1157
Lamers, H. J. G. L. M. 2005, in IAU Symp. 227, Massive Star Birth: A
   Crossroads of Astrophysics, ed. R. Cesaroni et al. (Cambridge: Cambridge
   Univ. Press), 303
Lamers, H. J. G. L. M., Beaulieu, J. P., de Wit, W. J., et al. 1999, A&A,
   341, 827
Lebouteiller, V., Bernard-Salas, J., Sloan, G. C., & Barry, D. J. 2010, PASP,
   122, 23
Leroy, A. K., Bolatto, A., Bot, C., et al. 2009, ApJ, 702, 352
Li, A., & Draine, B. T. 2002, ApJ, 576, 762
Luck, R. E., Moffett, T. J., Barnes, T. G., III, & Gieren, W. P. 1998, AJ,
Mainzer, A., Bauer, J., Cutri, R. M., et al. 2014, ApJ, 792, 30
Martin-Zaïdi, C., Augereau, J.-C., Ménard, F., et al. 2010, A&A, 516, A110
Mathis, J. 1990, AR
                     &A, 28, 37
Meatheringham, S. J., & Dopita, M. A. 1991, ApJS, 76, 1085
Meeus, G., Waters, L. B. F. M., Bouwman, J., et al. 2001, A&A, 365, 476
```

Meixner, M., Panuzzo, P., Roman-Duval, J., et al. 2013, AJ, 146, 62

```
Muzerolle, J., D?Alessio, P., Calvet, N., & Hartmann, L. 2004, ApJ, 617, 406
Najita, J., Carr, J. S., Glassgold, A. E., Shu, F. H., & Tokunaga, A. T. 1996,
   ApJ, 462, 919
Oliveira, J. M., van Loon, J. T., Sloan, G. C., et al. 2011, MNRAS, 411, L36
Oliveira, J. M., van Loon, J. T., Sloan, G. C., et al. 2013, MNRAS, 428, 3001
Palla, F., & Stahler, S. W. 1991, ApJ, 375, 288
Peeters, E., Hony, S., Van Kerckhoven, C., et al. 2002, A&A, 390, 1089
Peimbert, M., Peimbert, A., & Ruiz, M. T. 2000, ApJ, 541, 688
Richter, M. J., Jaffe, D. T., Blake, G. A., & Lacy, J. H. 2002, ApJL, 572, L161
Rodgers, A. W., Conroy, P., & Bloxham, G. 1988, PASP, 100, 626
Rubele, S., Pastorelli, G., Girardi, L., et al. 2018, MNRAS, 478, 5017
Ruffle, P. M. E., Kemper, F., Jones, O. C., et al. 2015, MNRAS, 451, 3504
Russell, S. C., & Dopita, M. A. 1992, ApJ, 384, 508
Sandstrom, K. 2014, HST Proposal, 13659
Sandstrom, K. M., Bolatto, A. D., Bot, C., et al. 2012, ApJ, 744, 20
Sewiło, M., Carlson, L. R., Seale, J. P., et al. 2013, ApJ, 778, 15
Sheets, H. A., Bolatto, A. D., van Loon, J. T., et al. 2013, ApJ, 771, 111
Siess, L., Dufour, E., & Forestini, M. 2000, A&A, 358, 593
Simon, J. D., Bolatto, A. D., Whitney, B. A., et al. 2007, ApJ, 669, 327
Skrutskie, M. F., Cutri, R. M., Stiening, R., et al. 2006, AJ, 131, 1163
Sloan, G. C., Herter, T. L., Charmandaris, V., et al. 2015, AJ, 149, 11
Sloan, G. C., Jura, M., Duley, W. W., et al. 2007, ApJ, 664, 1144
Sloan, G. C., Keller, L. D., Forrest, W. J., et al. 2005, ApJ, 632, 956
Sloan, G. C., Kraemer, K. E., Matsuura, M., et al. 2006, ApJ, 645, 1118
Sloan, G. C., Kraemer, K. E., Wood, P. R., et al. 2008, ApJ, 686, 1056
Smith, R. C. & MCELS Team 1998, PASA, 15, 163
Stanghellini, L., García-Lario, P., García-Hernández, D. A., et al. 2007, ApJ,
  671, 1669
Stephens, I. W., Gouliermis, D., Looney, L. W., et al. 2017, ApJ, 834, 94
Strom, K. M., & Strom, S. E. 1994, ApJ, 424, 237
Strom, S. E., Strom, K. M., Yost, J., Carrasco, L., & Grasdalen, G. 1972, ApJ,
Szewczyk, O., Pietrzyński, G., Gieren, W., et al. 2009, AJ, 138, 1661
Testor, G., Heydari-Malayeri, M., Chen, C.-H. R., et al. 2014, A&A, 564, A31
Thé, P. S., de Winter, D., & Perez, M. R. 1994, A&AS, 104, 315
Thé, P. S., Tjin, H. R. E., Steenman, H., & Wesselius, P. R. 1986, A&A,
  155, 347
Thi, W. F., van Dishoeck, E. F., Blake, G. A., et al. 2001, ApJ, 561, 1074
Tognelli, E., Prada Moroni, P. G., & Degl'Innocenti, S. 2011, A&A, 533,
  A109
van den Ancker, M. E., Meeus, G., Cami, J., Waters, L. B. F. M., &
  Waelkens, C. 2001, A&A, 369, L17
van den Ancker, M. E., Wesselius, P. R., & Tielens, A. G. G. M. 2000, A&A,
  355, 194
van Leeuwen, F. 2007, A&A, 474, 653
van Loon, J. T., Oliveira, J. M., Gordon, K. D., Sloan, G. C., &
  Engelbracht, C. W. 2010, AJ, 139, 1553
Vijh, U. P., Witt, A. N., & Gordon, K. D. 2005, ApJ, 633, 262
Vioque, M., Oudmaijer, R. D., Baines, D., et al. 2018, A&A, 620, A128
Ward, J. L., Oliveira, J. M., van Loon, J. T., & Sewiło, M. 2017, MNRAS,
  464, 1512
Weingartner, J. C., & Draine, B. T. 2001, ApJ, 548, 296
Winkler, P. F., Smith, R. C., Points, S. D. & MCELS Team 2015, in ASP Conf.
   Ser. 491, Fifty Years of Wide Field Studies in the Southern Hemisphere:
  Resolved Stellar Populations of the Galactic Bulge and Magellanic Clouds,
  ed. S. Points & A. Kunder (San Francisco, CA: ASP), 343
Wisniewski, J. P., Kowalski, A. F., Bjorkman, K. S., Bjorkman, J. E., &
  Carciofi, A. C. 2007, ApJL, 656, L21
Wright, E. L., Eisenhardt, P. R. M., Mainzer, A. K., et al. 2010, AJ, 140, 1868
Zaritsky, D., Harris, J., Thompson, I. B., Grebel, E. K., & Massey, P. 2002, AJ,
   123, 855
```